An energy preserving formulation for the simulation of multiphase turbulent flows.

Abstract

In this manuscript we propose an energy preserving formulation for the simulation of multiphase flows. The new formulation reduces the numerical diffusion with respect to previous formulations dealing with multiple phases, which makes this method to be especially appealing for turbulent flows. In this work we discuss the accuracy and conservation properties of the method in various scenarios with large density and viscosity jumps across the interface including surface tension effects.

1 Introduction

Nowadays the simulation of turbulent flows is the object of intense research. Although numerical techniques and models have been already widely investigated in the literature for single phase flows, current studies are still far from a complete understanding of real processes encountered in a countless number of applications involving multiple phases, such as rocket engines injectors, diesel engines or chemical process. When two or more different phases are present in the system we can distinguish not only a range of characteristic length-scales related to the turbulent nature of the flow , but also a range of sizes and shapes of each of the phases present in the system. This fact significantly increases the complexity of the simulations required to investigate such type of problems, which require a continuous development and optimization of the numerical techniques and models. The scientific community has made an important effort developing models for multiphase flows when one of the phases can be considered as disperse (only some examples can be found in [27, 11, 29]). However, the extension and evaluation numerical models to situations where the structures of the interfaces is well captured is less prolific. The development of these methods is important in order to evaluate the importance of turbulence in process where any of the multiple phases present on it can be considered as disperse.

Numerical techniques used for the simulation of turbulent flows and multiphase flows have been traditionally different. On one hand, numerical schemes typically used for the simulation of turbulent flows must pay an especial attention to the conservation of global properties such as energy. Because we usually want to solve for problems where the smallest scales of the flow cannot be solved

(e.g. Large Eddy Simulations) we need to introduce physical models to capture the correct behavior of the system on the resolved scales. Thus, in order to validate the physical models, it is desirable to reduce any numerical dissipation that can interfere with the performance of the subgrid models. On the other hand, the schemes presented for the simulation of multiple phases are designed to guarantee stability, although they try to reduce the numerical dissipation as much as possible [26].

The selection of the most suitable numerical scheme for the simulation of complex problems involving different phases is not simple. One must evaluate the pros and cons of each numerical scheme for the particular problem that needs to be solved. First of all, one has to be careful on the choice of the numerical method when dealing with multiphase flow with large density ratios [8]. The number of works coupling these methods with turbulent flows is still scarce. Desjardins et al [9] has proposed a level set/ghost fluid method for simulating turbulent atomization. More recently, Raessi & Pitch [24] have proposed a consistent mass and momentum transport using a level set method. In this work, we propose a new numerical scheme for the simulation of turbulent multiphase flows. The method is based on the discretization procedure followed by Verstappen et al [33, 34] for the simulation of single phase flows. This method has been shown to strictly conserve energy irrespective of the mesh resolution in those cases where there is not any physical mechanism of energy dissipation. Indeed, the method is derived in order to reduce numerical dissipation at expenses of the local truncation error. This type of methods has attracted the interest of the scientific community on the simulation of incompressible [33, 34] and compressible flows [1, 10, 15, 16], but it has not been extended to systems with multiple phases yet.

When dealing with multiple phases, one must choose the method to track the interface. Among all the methods available in the literature, the Volume Of Fluid (VOF) method seems especially suitable for the simulation of underresolved simulations because it enforces mass conservation and it handles natural topological changes at the interface in the subgrid level. We chose the Gerris Flow Solver [22, 23, 21] as a platform to implement the new numerical scheme. This code has been well validated for the simulation of multiphase flows in various problems involving interfaces [14, 13, 2]. Moreover, the method has been designed to reduce the appearance of *parasitic* currents induced by surface tension forces [23], which is an appealing characteristic of the numerical scheme if one wants to reduce any artificial energy dissipation/generation on the system.

This work is structured as follows. First, the basic equations are presented. Then the numerical method is described paying an especial attention to the problems that arise when we account for different phases with arbitrary density and viscosity jumps and also when surface tension effects are included.
Finally, we present different test cases to investigate the performance of the method in different situations.

2 Basic equations

The basic equations that need to be solved to multiphase incompressible flows are the Navier-Stokes equations [23],

$$\nabla \cdot \boldsymbol{u} = 0, \tag{1}$$

$$\partial_t c_i + \nabla \cdot (c_i \boldsymbol{u}) = 0, \tag{2}$$

$$\rho \left(\partial_t \boldsymbol{u} + \boldsymbol{u} \cdot \nabla \boldsymbol{u}\right) + \nabla p - \nabla \cdot \left(2\mu \boldsymbol{D}^T\right) - \sigma \kappa \delta_s \boldsymbol{n} = 0, \tag{3}$$

where $\boldsymbol{u}$ is the fluid velocity vector, c_i is the volume fraction of the ith component present in the system, p is the fluid pressure, $\boldsymbol{D}^T$ is the deformation tensor defined as $D^T_{ij} = (\partial_i u_j + \partial_j u_i)/2$, σ is the surface tension coefficient, κ is the curvature of the interface, $\boldsymbol{n}$ is the normal to the interface and δ_s is the Dirac distribution function which is used to express that the surface tension term is concentrated on the interface. The density ρ and viscosity μ represent the averaged fluid properties.

3 Numerical scheme

In this section we describe the numerical scheme developed in this work for the simulation of turbulent multiphase flows. The scheme presented here can be seen as an extension of the previous works presented by Verstappen et al [33, 34] for the simulation of turbulence flows in order to extend the applicability of the scheme to multiple phases. using the Volume Of Fluid techniques (VOF) implemented in Gerris [22, 23].

3.1 Skew symmetric formulation for structured meshes

The underlying idea of the skew-preserving formulations is that the discretization scheme must satisfy certain properties in order to preserve mass and energy. Such properties are satisfied at expenses of increasing the local truncation error with respect to other formulations. In incompressible fluids, mass conservation is typically imposed by satisfying condition (1) for the velocity field at each time step. However, this condition is not sufficient to guarantee conservation of other properties such as the total energy. In the absence of thermal effects, the only energy present in the system is the mechanical energy, defined as $E_m = \frac{1}{2}\rho|\boldsymbol{u}|^2$. The evolution of the mechanical energy can be obtained by scalar multiplication of Eq. 3 with the velocity field,

$$\boldsymbol{u} \cdot \left(\rho \left(\partial_t \boldsymbol{u} + \boldsymbol{u} \cdot \nabla \boldsymbol{u}\right) + \nabla p - \nabla \cdot \left(2\mu \boldsymbol{D}^T\right) - \sigma \kappa \delta_s \boldsymbol{n}\right) = 0, \tag{4}$$

which can be written as

$$\partial_t E_m + \nabla \cdot (E_m \boldsymbol{u}) = \nabla \cdot (\boldsymbol{\tau} \boldsymbol{u}) - \phi_v - \boldsymbol{S} \cdot \boldsymbol{u} \tag{5}$$

where $\boldsymbol{\tau}$ is the total stress tensor, ϕ_v is the viscous dissipation function and $\boldsymbol{S}$ is the source term, that includes surface tension effects. From the mathematical point of view it can be proved that, for an inviscid fluid without any external force, the evolution of the total system's energy is strictly zero because the following two fundamental properties of the continuous differential operators hold [33],

$$(\boldsymbol{u} \cdot \nabla)' = -(\boldsymbol{u} \cdot \nabla), \tag{6}$$

$$\nabla' = \nabla, \tag{7}$$

where the asterisk represents the transpose. Based on these properties for the continuous operators, Verstappen et al [33] have presented a 2nd and 4th order conservative scheme for inviscid fluids by forcing the discrete operators to satisfy conditions (6) and (7). Interestingly, this formulation has been developed for an arbitrary non-uniform structured grids.

3.1.1 Temporal discretization

As stated above, the numerical scheme proposed in this work must satisfy energy conservation, but there are other properties that ideally one must satisfy when dealing with multiphase turbulent flows. For example, we want the method to be stable and fast in order to perform simulations of complex problems where the computational time determines the capabilities of the code. In addition, we want the method to reduce the *parasitic* currents induced by the numerical method when surface tension effects are included. One must keep in mind all these properties when equations (1)-(3) are discretisized in time. Following Verstappen et al [33], the system of equations (1)-(3) can be discretised in time by introducing a time step δt and using a modified leapfrog method of the form

$$\boldsymbol{M} \boldsymbol{u}_h^{n+1} = 0, \tag{8}$$

$$\boldsymbol{\Omega} \frac{\boldsymbol{u}_h^{n+\beta+1/2} - \boldsymbol{u}_h^{n+\beta-1/2}}{\delta t} + \boldsymbol{C}(\boldsymbol{u}_h^{n+\beta}) \boldsymbol{u}_h^{n+\beta} + \boldsymbol{D} \boldsymbol{u}_h^{n+\beta} - \boldsymbol{M}' \boldsymbol{p}_h^{n+\beta} + \boldsymbol{S}^{n+\beta} = 0, \tag{9}$$

where $\boldsymbol{M}$ is a matrix representing the discretization of the divergence operator, $\boldsymbol{u}_h^n$ and $\boldsymbol{p}_h^n$ are the discrete velocity and pressure function vector at time $t = n\delta t$, $\boldsymbol{\Omega}$ is the diagonal matrix containing the area (in 2D) or volume (in 3D) of the volume of control used for the discretization, the matrix $\boldsymbol{C}(\boldsymbol{u})$ represents the discretization of the convective operator, $\boldsymbol{D}$ contains the matrix coefficients of the discretization of the diffusive term and $\boldsymbol{S}$ represents the surface tension term. In this method, the intermediate velocities are obtained as

$$u_h^{n+\beta} = (1+\beta) u_h^n - \beta u_h^{n-1}, \tag{10}$$

$$u_h^{n+\beta+1/2} = \left(\beta + \frac{1}{2}\right) u_h^{n+1} - \left(\beta - \frac{1}{2}\right) u_h^n. \tag{11}$$

The system of Eqs. (8)-(9) is solved using a classical time-splitting projection method [4], which gives,

$$\boldsymbol{\Omega}\frac{\left(\beta+\frac{1}{2}\right)\boldsymbol{u}^{*}-2\beta\boldsymbol{u}^{n}+\left(\beta-\frac{1}{2}\right)\boldsymbol{u}^{n-1}}{\delta t}+\boldsymbol{C}(\boldsymbol{u}^{n+\beta})\boldsymbol{u}^{n+\beta}=-\boldsymbol{D}\boldsymbol{u}_{h}^{n+\beta}-\boldsymbol{S}^{n+\beta}, \quad (12)$$

$$\boldsymbol{u}^{n+1}=\boldsymbol{u}^{*}-\frac{\delta t}{\rho^{n+\beta}}\nabla p^{n+\beta}. \quad (13)$$

The right hand term in Eq. (12) groups the terms associated with viscosity and surface tension. This type of discretization, while interesting to guarantee energy conservation, it is not convenient to apply classical methods devised to minimize the appearance of *parasitic* currents induced by surface tension. For that reason, inspired by the temporal splitting techniques presented by [17, 30], we propose a modified discretization of the type

$$\boldsymbol{\Omega}\frac{\left(\beta+\frac{1}{2}\right)\boldsymbol{u}^{*}-2\beta\boldsymbol{u}^{n}+\left(\beta-\frac{1}{2}\right)\boldsymbol{u}^{n-1}}{\delta t}+\boldsymbol{C}(\boldsymbol{u}^{n+\beta})\boldsymbol{u}^{n+\beta}=-\boldsymbol{D}\boldsymbol{u}_{h}^{n+\beta}, \quad (14)$$

$$\boldsymbol{\Omega}\frac{\boldsymbol{u}^{**}-\boldsymbol{u}^{*}}{\delta t}=-\boldsymbol{S}^{n+\beta} \quad (15)$$

$$\boldsymbol{u}^{n+1}=\boldsymbol{u}^{**}-\frac{\delta t}{\rho^{n+\beta}}\nabla p^{n+\beta}. \quad (16)$$

The main advantage of this scheme is that, like the original Verstappen formulation, it preserves energy for single phase flows. In addition, it is straightforward to implement the method implemented in Gerris and described in [23] to completely remove *parasitic* currents for a droplet in equilibrium. This method is further described below.

In situations with two phases with different viscosities and densities, we need to define the physical properties as a function of the color function

$$\rho^{n+\beta}=f_1(\tilde{c}^{n+\beta},\rho_1,\rho_2) \quad (17)$$

$$\mu^{n+\beta}=f_2(\tilde{c}^{n+\beta},\mu_1,\mu_2) \quad (18)$$

where $\tilde{c}^{n+\beta}$ is a filtered variable of the color function $c^{n+\beta}$, which is obtained solving for the advection equation

$$\frac{\boldsymbol{c}_h^{n+\beta}-\boldsymbol{c}_h^{n+\beta-1}}{\delta t}+\boldsymbol{M}(\boldsymbol{u}_h^{n-1/2+\beta}\boldsymbol{c}_h^{n-1/2+\beta})=0. \quad (19)$$

We emphasize that the filtering is applied at every time step based on the position of the reconstructed interface obtained from $\boldsymbol{c}_h$. This filter function turns to be an important parameter to improve the convergence of the Poisson solver for large density ratios. For the simulations included in this work, the filter is applied in a range of 2-3 cells across the interface. This equation is solved using the VOF geometrical advection subroutines implemented in Gerris and described in detail for octree meshes in [23]. The most accurate form of

the functions (17)-(18) depends on the problem considered. A discussion of the most standard expressions can be found in [32]. For simplicity, in this work we only consider expressions of the form

$$\begin{aligned} \rho^{n+\beta} &= \tilde{c}^{n+\beta}\rho_1 + (1-\tilde{c}^{n+\beta})\rho_2 \\ \mu^{n+\beta} &= \tilde{c}^{n+\beta}\mu_1 + (1-\tilde{c}^{n+\beta})\mu_2 \end{aligned} \tag{20}$$

We emphasize that this formulation incorporates a parameter β that must be determined. Verstappen et al [33] proposes $\beta = 0.05$ for single phase flows. In this work, we will use well established tests for multiphase fluids in order to calibrate this parameter.

3.1.2 Spatial discretization

In this work we have adopted the 2nd order scheme described in [33]. The main advantage of a 2nd order formulation with respect to higher order methods is that it allows for a relatively simple extension to octrees and Adaptive Mesh Refinement Techniques (AMR) implemented in Gerris [22, 23, 21], for which the derivation of 4rd order schemes for a general case is a cumbersome work. The description and investigation of the proposed scheme for octrees is currently being investigated.

The method is presented for a staggered grid and two dimensions but it has been implemented in both, two and three dimensions. Details about the extension of the numerical scheme to octree meshes are given in the next section.

Advection term

The discretization for the advection term can be obtained by discretising the momentum equation in a region $\Omega_{i+1/2,j} = [x_{i-1/2}, x_{i+1/2}] \times [y_{j-1}, y_j]$. We use the notation shown in Figure 1.

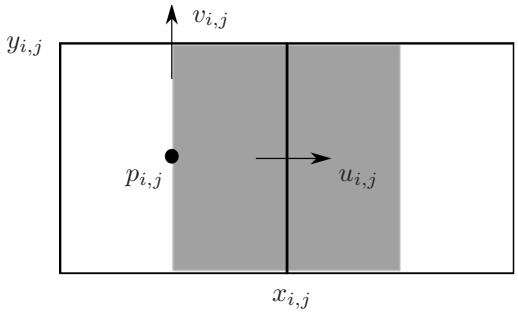

Fig. 1: Notation convection for the pressure, velocity and position of the cell (i, j). The shaded region represents the control volume used to discretize the momentum equation in the x-direction.

A detailed derivation of the discretization scheme for single phase flows can be found in [33]. Here, we briefly summarize the procedure followed to obtain the discrete form. The two dimensional version for the discretized transport equation in absence of viscosity and surface tension can be expressed as [33]

$$\begin{aligned}\Omega_{i+1/2,j}\frac{du_{i,j}}{dt} &+ \frac{1}{2}\left(\overline{u}_{i+1/2,j}+\overline{v}_{i+1/2,j}-\overline{u}_{i-1/2,j}-\overline{v}_{i+1/2,j-1}\right)u_{i,j}\\ &+ \frac{1}{2}\overline{u}_{i+1/2,j}u_{i+1,j}-\frac{1}{2}\overline{u}_{i-1/2,j}u_{i-1,j}+\frac{1}{2}\overline{v}_{i+1/2,j}u_{i,j+1}-\frac{1}{2}\overline{v}_{i+1/2,j-1}u_{i,j-1}=0,\end{aligned} \tag{21}$$

$$\begin{aligned}\Omega_{i+1/2,j}\frac{dv_{i,j}}{dt} &+ \frac{1}{2}\left(\overline{v}_{i,j+1/2}+\overline{u}_{i,j+1/2}-\overline{v}_{i,j-1/2}-\overline{u}_{i-1,j+1/2}\right)v_{i,j}\\ &+ \frac{1}{2}\overline{v}_{i,j+1/2}v_{i,j+1}-\frac{1}{2}\overline{v}_{i,j-1/2}v_{i,j-1}+\frac{1}{2}\overline{u}_{i,j+1/2}v_{i+1,j}-\frac{1}{2}\overline{u}_{i-1,j+1/2}v_{i-1,j}=0,\end{aligned} \tag{22}$$

where the overbar velocities are used to denote the mass flux through the faces, which are related to the face velocities using the mid-point rule

$$\overline{u}_{i,j} = (y_j - y_{j-1})u_{i,j}, \tag{23}$$

$$\overline{v}_{i,j} = (x_i - x_{i-1})v_{i,j}. \tag{24}$$

Note that in the case of fluxes across the control volume used to discretize the momentum equation, it is imperative to interpolate the fluxes with constant weights. For instance,

$$\overline{u}_{i+1/2,j} = \frac{1}{2}\left(\overline{u}_{i+1,j}+\overline{u}_{i,j}\right), \tag{25}$$

$$\overline{v}_{i+1/2,j} = \frac{1}{2}\left(\overline{v}_{i+1,j}+\overline{v}_{i,j}\right). \tag{26}$$

These relations allow us to write the momentum equation in vector notation as follows

$$\boldsymbol{\Omega}\frac{d\boldsymbol{u}_h}{dt} + \boldsymbol{C}(\overline{\boldsymbol{u}})\boldsymbol{u}_h = 0 \tag{27}$$

where the overbar has been used to denote the volumetric flux and $\boldsymbol{C}$ is the discrete convective operator obtained upon substitution of the interpolated fluxes into Eqs. 21-22 . Based on the equation above it can be proved that the evolution of the discrete energy of the system, defined as $\boldsymbol{u}_h'\boldsymbol{\Omega}\boldsymbol{u}_h$, obeys [33]

$$\frac{d\boldsymbol{u}_h'\boldsymbol{\Omega}\boldsymbol{u}_h}{dt} = -\boldsymbol{u}_h'\left(\boldsymbol{C}(\overline{\boldsymbol{u}})+\boldsymbol{C}'(\overline{\boldsymbol{u}})\right)\boldsymbol{u}_h, \tag{28}$$

which, for inviscid fluids and in absence of surface tension, is satisfied if only if $\boldsymbol{C}(\overline{\boldsymbol{u}})$ is skew-symmetric. As proved by [33], this condition imposes that the interpolation weights for the discrete velocities and also mass fluxes must be constant.

We remark that the condition above is automatically satisfied for any arbitrary density jump. This facts makes extremely important to accurately transport the concentration field of each of the color function. Inconsistencies between the velocity advection and interface advection can lead to the appearance of numerical instabilities. We will show that indeed this point is extremely important in order to investigate the performance of the method.

Diffusion term

The diffusion term is discretised obtaining the proper expressions for the diffusive operator $-\nabla\cdot\nabla$. To do that, we denote as $\boldsymbol{M}$ the discretization of the divergence operator such that, neglecting any effect of the boundary conditions,

$$\boldsymbol{M}\boldsymbol{u}_h = 0. \tag{29}$$

Now we impose that the following condition,

$$(\nabla p, \boldsymbol{u}) = -(p, \nabla\cdot\boldsymbol{u}), \tag{30}$$

must be also satisfied in the discrete form. If we approach the discrete pressure gradient as $\boldsymbol{G}p_h \approx \nabla p$, then Eq. 30 establishes that the discrete operators should satisfy

$$(\boldsymbol{G}p_h)'\boldsymbol{\Omega}\boldsymbol{u}_h = -p_h\boldsymbol{M}\boldsymbol{u}_h, \tag{31}$$

which is always true if the discrete gradient operator is defined as

$$\boldsymbol{G} = -\boldsymbol{\Omega}^{-1}\boldsymbol{M}'. \tag{32}$$

Because we work with a staggered grid, the control volumes for the u and v components (in 2D) differ and the approximation obtained for the Laplacian, $-\boldsymbol{M}\boldsymbol{\Omega}^{-1}\boldsymbol{M}^*$, can not be applied here. Instead, the diffusive fluxes through the control volume faces must be obtained separately for each component. For instance, for the u component, the surface integrals of the diffusive fluxes F^{diff} through control volume defined by $\boldsymbol{\Omega}_{i+1/2,j}$, can be written as

$$\frac{1}{\rho_{i+1/2,j}}\left[(\overline{F_x^{\text{diff}}})_{i+1/2,j} - (\overline{F_x^{\text{diff}}})_{i-1/2,j} + (\overline{F_y^{\text{diff}}})_{i,j} - (\overline{F_y^{\text{diff}}})_{i,j-1}\right]. \tag{33}$$

where $\rho_{i+1/2,j}$ represents the averaged density in the control volume inside $\boldsymbol{\Omega}_{i+1/2,j}$ obtained from the evaluation of the filtered color function at the center of the volume of control considered to discretize the momentum equation. Following [33], the surface integrals are approximated as

$$(\overline{F_x^{\text{diff}}})_{i+1/2,j} = \Delta_{i,j}(F_x^{\text{diff}})_{i+1/2,j},$$
$$(\overline{F_y^{\text{diff}}})_{i,j} = \Delta_{i+1/2,j}(F_y^{\text{diff}})_{i,j},$$

where we have exploited the fact that in octree meshes the mesh size, Δ_i is constant for all dimensions and, we have defined $\Delta_{i+1/2,j} = (\Delta_{i,j} + \Delta_{i+1,j})/2$.

Finally, we discretize the diffusive flux using the proper gradient operator defined for the coordinate considered and taking into account both, viscosity and density changed. Thus we obtain

$$(F_x^{\text{diff}})_{i+1/2,j} = \mu_{i+1,j} \frac{u_{i+1,j} - u_{i,j}}{\Delta_{i+1,j}} \tag{34}$$

$$(F_y^{\text{diff}})_{i,j} = \mu_{i+1/2,j} \frac{u_{i,j+1} - u_{i,j}}{\Delta_{i,j+1/2}} \tag{35}$$

Surface tension term

Surface tension is incorporated in the formulation by exploiting the equality obtained from the momentum equation in absence of motion,

$$\nabla p = \sigma \kappa \nabla c \tag{36}$$

where σ is the surface tension coefficient, κ is the curvature and c is the color function used to define each of the phases.

Following the procedure used in the current implementation in Gerris, surface tension terms are incorporated by adding the source term effects before the projection step as

$$u^{**} = u^* + \frac{\delta t \sigma \kappa^{n+\beta}}{\rho^{n+\beta}} \nabla c^{n+\beta} \tag{37}$$

where the gradient is formally approximated using Eq. (32). Thanks to the fact that the pressure gradient and color function gradient is discretized with the same operator, condition (36) also holds numerically and both terms balance in the case of a droplet or bubble in equilibrium. This scheme, proposed by [25, 12, 28] minimize the appearance of *parasitic* currents, that have been checked to be strictly zero for a droplet in equilibrium with the surrounding liquid. More details about the implementation of the surface tension terms in octrees can be found in [22, 23].

Discretization of the Poisson equation

Finally the projection method requires to discretize the Poisson equation

$$\nabla \cdot \left(\frac{\delta t}{\rho^{n+\beta}} \nabla p^{n+\beta} \right) = \nabla \cdot \boldsymbol{u}^{**}. \tag{38}$$

As explained above, the symmetry properties of the continuous operators are satisfied also in the discrete form by approaching the Laplacian operator by $-\boldsymbol{M}\boldsymbol{\Omega}^{-1}\boldsymbol{M}^*$. This equation is solved using the native multigrid solver implemented in Gerris and described in [22].

VOF advection

For practicity, we solve for the advection equation using the functions readily available in Gerris [22, 23, 21], which uses a VOF method that ensures mass conservation in the discrete form. The advection equation in two steps, namely, interface reconstruction and geometrical flux computation and interface advection. Further details about the methods implemented in Gerris can be found in [22, 23]. One must keep in mind that this method is designed to advect interfaces that are properly resolved. The direct application of this method is not capable to solve properly the advection of small fragments or structures at the interface whose characteristic length become of the order of the grid size. For this reason, we expect the method to perform better in those cases where the interface is well resolved. Either improved methods to reproduce the behavior of the interface in the subgrid scale (e.g. lagrangian methods) or alternative methods to track the interface may be implemented in the proposed formulation.

4 Test cases

4.1 The Green Taylor vortex

In order to show the performance of the scheme proposed in terms of convergence and energy conservation in single phase flows we solve for the Green Taylor vortex in an inviscid fluid. This test allows us to verify the original implementation proposed by Verstappen et al [33] in terms of energy conservation and accuracy. Because we know the analytical solution

$$U = -\cos(2\pi x)\sin(2\pi y)), \tag{39}$$

$$V = \sin(2\pi x)\cos(2\pi y), \tag{40}$$

we can measure the accuracy of the results in a domain with $L = 1$ at $t = 1$. We use the L_2 norm to measure how the global error behaves and the L_∞ norm to evaluate the importance of the local error.

Figure 2(a) shows that, as proved by [18], the method is exactly second order for uniform meshes in both L_2 and L_∞ norms. It is remarkable the good energy conservation properties of the scheme in all cases (Figure 2(b)), where energy is preserved within machine accuracy.

4.2 Two-dimensional rising bubble

In order to test the performance of the method in flows with multiple phases we consider the following problem. A single bubble with diameter $D = 2/3$ is placed at $(0, 0)$ inside a rectangular domain with dimensions $L/D = [-1.5 : 1.5, -1.5 : 3]$. The gas density is set to $\rho_g = 1.226$ and the liquid density is $\rho_l = 1000$. Gravity ($g = -9.81$) and surface tension effects ($\sigma = 728$) are included. In this case, the bubble ascension and deformation is controlled by

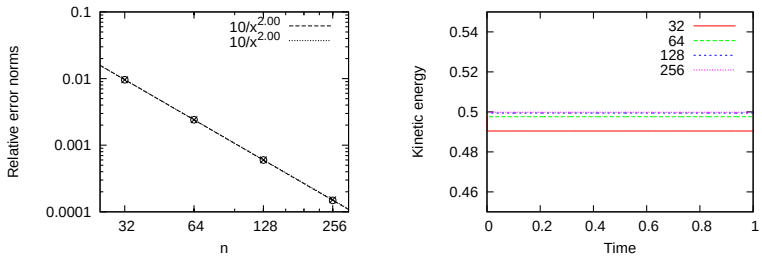

(a) L_2 and L_∞ norm for different grid points.

(b) System's kinetic energy

Fig. 2: Green-Taylor vortex. Left: error norms measured at $t = 1$ for a uniform grid as a function of the number of points per direction n (symbol x is used for the L_2 norm and $\odot$ is used for the L_∞ norm). Right: Temporal evolution of the kinetic energy as a function of the level of refinement.

buoyancy and tension forces. The most representative nondimensional number is the Bond number

$$\mathrm{Bo} = \frac{\rho_l g D^2}{\sigma} = 5.983. \tag{41}$$

This problem has been discussed by [12] and later used by Popinet [23] as a validation of the surface tension implementation. In this work this test case is used to discuss the value of the parameter β and to discuss the accuracy of the proposed numerical scheme in under-resolved simulations involving two different phases.

Figure (3) compares the interface shape obtained with with standard advection scheme implemented in Gerris and that obtained with different values of β with the new advection scheme. We remark that for well resolved simulations, we expect both schemes to recover the same solution. The simulation converges for $D/\Delta = 85$ (Figure 3(a)). Among the different values of β tested here, Figure 3(b) reveals that the best fitting is obtained for $\beta = 0.15$ for all intermediate times considered in [12, 23] (Figure 3(c)). A priori, we have not found a rigorous explanation about why this value provides the most accurate results but as it will be shown, this value also provides the most accurate results for the oscillation of an inviscid droplet included below.

4.3 Oscillation of an inviscid droplet

The previous section has investigated the properties of the proposed numerical scheme in terms of energy conservation. In this section we evaluate the accuracy of the surface tension implementation. Although the current method is not designed to minimize the local error, it is interesting to have an idea of the accuracy of the scheme to capture the structures appearing at the interface

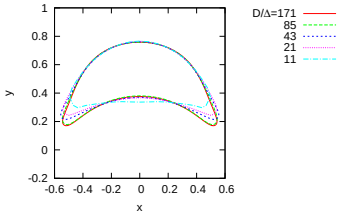

(a) Grid convergence of the skew symmetric formulation ($\beta = 0.15$)

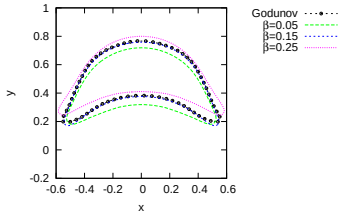

(b) Bubble shape obtained with the Bell-Cotella-Glaz (BCG) advection scheme implemented in Gerris [23] and with the skew-symmetric formulation for different values of β.

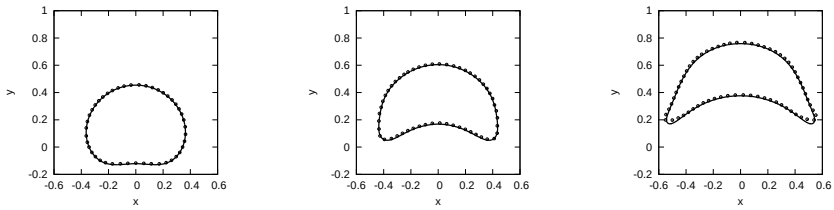

(c) Bubble shape at t=0.2,0.35 and 0.5 obtained at the larges resolution ($D/\Delta = 171$) with the BCG scheme implemented in Gerris ($\odot$) and with the skew symmetric formulation for $\beta = 0.15$ (-)

Fig. 3: Two-dimensional rising bubble at t=0.5. Bo = 5.983.

between two fluids.

We consider a two dimensional circular droplet of radius $r_0 = 0.1$ in a periodic box of length $L_{\text{box}}/r_0 = 10$. The droplet interface is initially perturbed such that

$$r(\theta) = r_0(1 + \alpha \cos(n\theta)). \tag{42}$$

As shown by [31], the oscillation frequency of the interface is given by

$$\omega_n^2 = \frac{(n^3 - n)\sigma}{(\rho_l + \rho_g)r_0^3}. \tag{43}$$

For the simulations contained in this section, $n = 2$, $\sigma = 1$, $\alpha = 0.025$, $\rho_l = 1$ and $\rho_g = 10^{-3}$.

Figure 4 depicts the temporal evolution of the system's energy for different mesh resolutions. We note that the system's kinetic energy oscillates with frequency $2\omega_n$. The frequency of the kinetic energy oscillation matches relatively well the one predicted by Eq. (43) and the energy dissipation is almost negligible. We note here that the accuracy of the results turn out to be sensible to the user-defined parameter β which has been introduced in the temporal discretization. Like in the previous independent test, the most accurate results

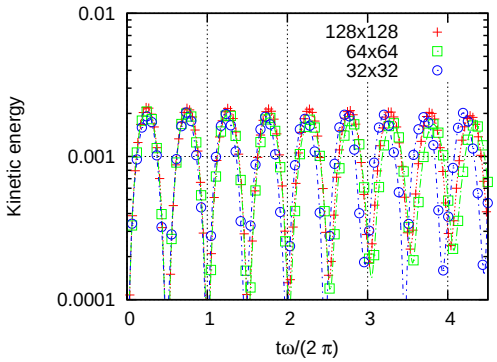

Fig. 4: Oscillation of an inviscid droplet: Temporal evolution of the kinetic energy obtained with the skew-symmetric formulation with $\beta = 0.15$. The oscillation period math well with the theoretical frequency.

Nodes	Relative error at $t = 4$
32^2	0.0200
64^2	0.0175
128^2	0.0075

Tab. 1: Oscillation of an inviscid droplet: Relative error of the time of 8th minimum on the system's kinetic energy of Figure 4 as a function of the level of refinement.

have been obtained for $\beta = 0.15$, for which the values obtained converge well to the theoretical value (Table 1). Other values ranging from 0.05 to 0.30 induce errors in the interface oscillation that have been shown to be less that 10 % in the examples considered in this work.

4.4 An inviscid droplet moving through an inviscid gas

The test cases above have allowed us to investigate the perfomance of the method in terms of accuracy, but not in terms of energy dissipation. In this section we evaluate the numerical dissipation of the scheme when dealing with multiphase flows by looking at the total energy in a two dimensional periodic box with two different inviscid phases. In particular, we consider a two-dimensional cilinder with radius $R/L_{box} = 0.2$ and density $\rho_l = 1000$ which is initialized with $U = 1$. The light phase, $\rho_g = 1$, is initially at rest. Similar cases, but with a higher density ratio, has been considered by Raessi & Pitsch [24].

As depicted in Figure 5, energy is well preserved even for the large density ratios tested here. However, in a general case, these conservation properties and

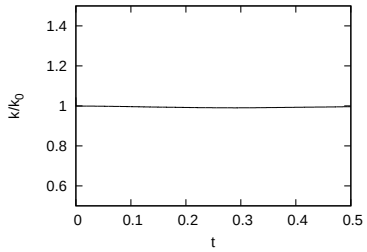

Fig. 5: Temporal evolution of the kinetic energy in a two-dimensional periodic box of an inviscid droplet with $U_0 = 1$ in an inviscid gas initially at rest. $r = \rho_l/\rho_g = 10^3$ $\sigma = 0$.

more in general the stability properties of the method have been shown to be influenced by the topological evolution of the interface. When, as in this case, both phases are correctly resolved the accuracy and the conservation properties of the numerical scheme are similar to those obtained for single flow fluids irrespective of the density ratio. As soon as under-resolved structures appear, the method has difficulties to preserve energy and for large density ratios, the method can become unstable for inviscid flows. The main reason for that is that when multiple phases are considered, energy conservation is determined not only by the solution of the momentum equation, but also by the solution of the advection equation for the VOF tracer. Indeed, we have observed that when the structures at the interface are not well resolved, energy conservation is mainly influenced by the advection method used for the tracer. The relevance of this feature of the method for practical applications is limited, given that as it will be shown in the next example, real flows are usually viscous and energy dissipation has been shown to be more relevant that the energies disturbances induced by this numerical method. In addition, one can partially circumvail the problem of under-resolved structure by modeling the disperse phase with continuum or lagrangian models that would allow to avoid the errors in those regions when one of the phases is not correctly resolved.

Figure 6 depicts the shape's interface obtained with the proposed scheme for different grid resolutions. For reference, we also include the solution obtained with the BCG advection scheme. This scheme has been proved to correctly capture the Kelvin-Helmholtz instability at large Reynolds numbers [2]. The solution is compared to the translation of a circle at the initial velocity. Due to the velocity boundary layer appearing at the interface in the discrete solution, Kelvin-Helmholtz instabilities develop at the droplet interface generating small droplets that become of the order of the grid size. This fact turns out to be a serious drawback when using this test to measure accuracy. Given the inviscid nature of the flow, there is not exist a unique solution and therefore one can only check the performance of the method in terms of global conservation properties.

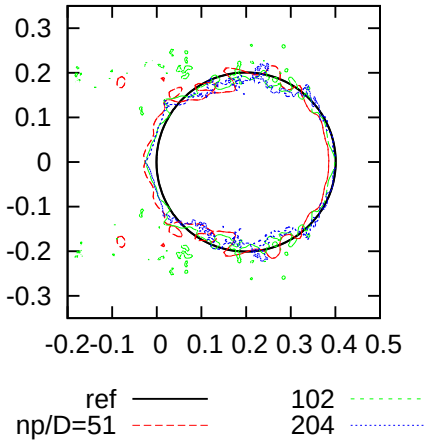

(a) Skew symmetric.

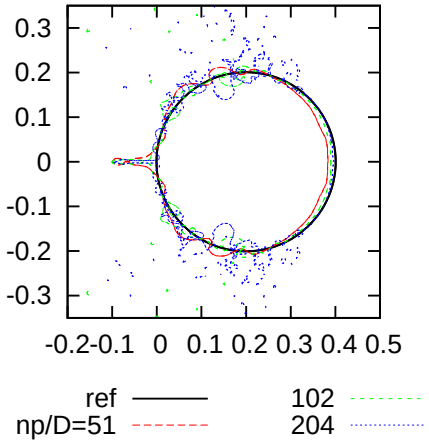

(b) BCG advection scheme

Fig. 6: Temporal evolution of the kinetic energy in a two-dimensional periodic box of an inviscid droplet with $U_0 = 1$ in an inviscid gas initially at rest. $r = \rho_l/\rho_g = 10^3$ $\sigma = 0$ $\mu = 0$.

In any event, as expected, the large density ratio between the two phases makes the deformation of the droplet not significant.

4.5 Energy decay in isotropic turbulence

4.5.1 Energy decay in isotropic turbulence for single phase flows

In order to test the performance of the current algorithm to simulate turbulent flows we consider the test case used by Meyers et at [19]. We measure the evolution of the kinetic energy in periodic box initialized with a velocity field corresponding to a given turbulent spectrum. Briefly, the procedure followed to to initialize the velocity field is as follows. We generate a random velocity field in Fourier space taking a random phase and an amplitude equal to one. The random velocity field is projected to obtain a solenoidal field following [20] and we rescale the spectra according to

$$E(k) = \alpha \epsilon^{2/3} k^{-5/3} f_L(kL_{\text{int}}) f_\nu(kL_{\text{int}} \text{Re}_L^{-3/4}) \tag{44}$$

where k is the wavenumber, α is a constant, ϵ is the dissipation rate L_{int} is the integral length and Re_L the Reynolds number defined as

$$\text{Re}_L = \frac{\sqrt{\int_0^\infty E(k)dk} L_{\text{int}}}{\nu} \tag{45}$$

We chose as characteristic velocity the square root of the kinetic energy which is fixed to 0.5,

$$k = \int_0^\infty E(k)dk = 0.5, \tag{46}$$

and the integral length is chosen as a characteristic lenghtscale. Following [19], for the simulations included here we choose $L_{\text{int}} = 0.5 L_{\text{box}} = 0.5$. Periodic boundary conditions are applied in all the domain boundaries

Meyers et at [19] have shown that, with spectral codes, it is possible to perform a DNS for a Reynolds number up to 375 for a uniform grid of 256^3 nodes. Figures 7(a)-7(c) show the results of the current numerical scheme for different grid resolutions for the kinetic energy decay and the evolution of the Taylor scale, λ, which is defined and

$$\frac{1}{\lambda^2} = \frac{1}{u'^2} \overline{\left(\frac{\partial u}{\partial x}\right)^2} \tag{47}$$

As expected, the energy decays and the Taylor microscale increases as the energy is dissipated. The results converge for a grid size of 256^3 which is in agreement with the maximum Reynolds numbers obtained by Meyers et at [19] with a similar grid. The results are also in agreement with those obtained from the free spectral code developed by S. Chumakov [5] (for further details read Refs. [6, 7] and references therein). For instance, Figure 8 shows the good agreement between the energy spectrum obtained with both codes at the final time.

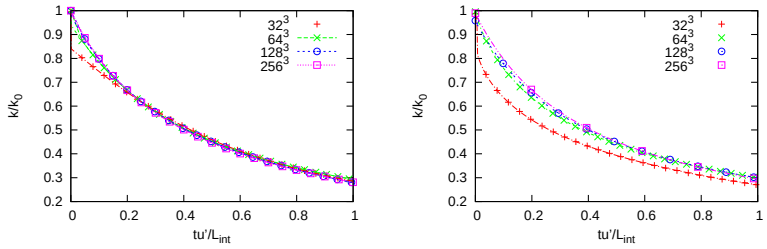

(a) System's kinetic energy (skew symmetric)

(b) System's kinetic energy (BCG)

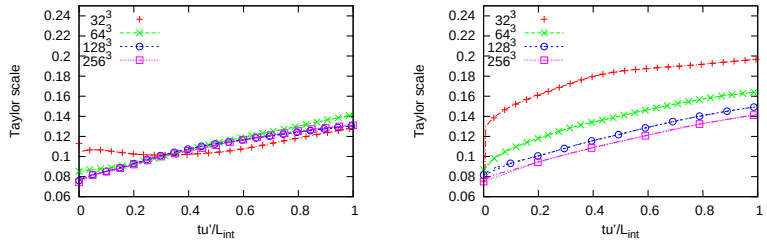

(c) Taylor's scale (skew symmetric)

(d) Taylor's scale (BCG)

Fig. 7: Temporal evolution of the system's kinetic energy and Taylor's scale as a function of the level of refinement for $\mathrm{Re}_L = 375$ for the skew symmetric formulation (left) and the BCG advection scheme (right).

For reference, we also show the results obtained with the Bell-Cotella-Glaz scheme (BCG) implemented in Gerris [3, 22, 23] (Figures 7(b)-7(d)). Although both schemes converge to the same solution as the mesh is refined, the quality of the solution in under-resolved simulations is significantly improved compared to non-energy-conservative schemes. Taking the solution of the finest grid as reference solution, Figures 9(a)-9(b) depicts the convergence rate for relative error defined as

$$\text{Relative Error} = \frac{\int_0^1 |Y - Y_{\text{fine}}| dt^*}{\int_0^1 Y dt^*}, \tag{48}$$

where $t^* = tu'/L_{\text{int}}$ and Y represents respectively k and λ. As clearly seen, the conservative scheme is especially important in order to obtain an accurate estimation of the Taylor scale, where the error with the skew preserving simulation in the 32^3 mesh is reduced about factor 10. The predictions of the energy decay turn out to be also more precise with the proposed formulation. This comparison strengthen the ultimate goal of this formulation: by minimizing the energy dissipation induced by the numerical method, the quality of the solution is significantly improved in under-resolved simulations. This aspect is expected to be critical when coupling subgrid models based on physical backgrounds,

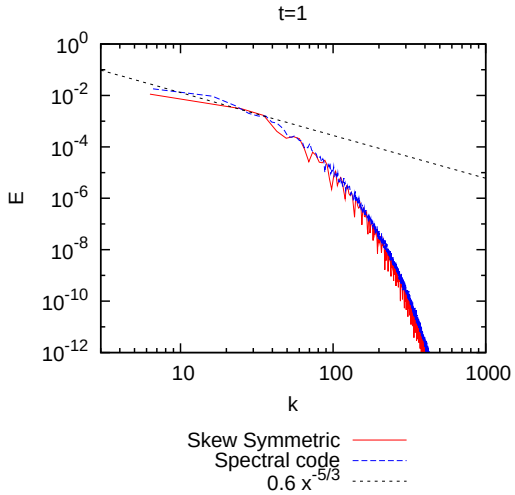

Fig. 8: Energy spectrum obtained from numerical simulation at t=1 with the skew symmetric formulation and a spectral code [5]. Grid: 256^3 cells.

where one may want to avoid any numerical artificial dissipation.

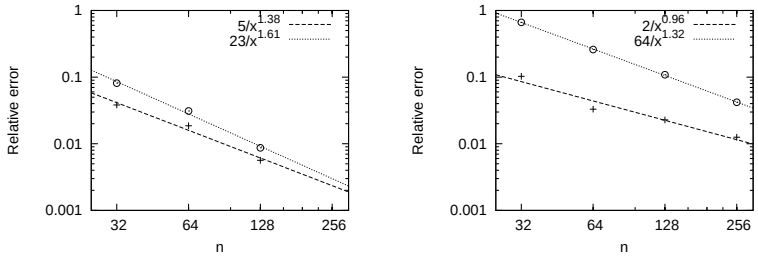

(a) Skew Symmetric (b) BCG

Fig. 9: Relative errors obtained for the kinetic energy (+) and the Taylor scale ($\odot$) as a function of the level of refinement for the skew symmetric formulation (left) and the BCG advection scheme (right).

4.5.2 Energy decay in isotropic turbulence with multiple phases

In this section we consider the analogous problem of the preceeding section when multiple phases are considered. A cilinder of radius $R/L_{\text{box}} = 0.1$ of dense phase with density ρ_l that is initially placed at the center of the box as depicted in

Figure 10(a), and a light fluid with density ρ_g. For convenience, we consider cases where the kinematic viscosity is equal in both fluids, so that we can define a unique $\mathrm{Re}_L = 375$ that corresponds to that tested for a single flow.

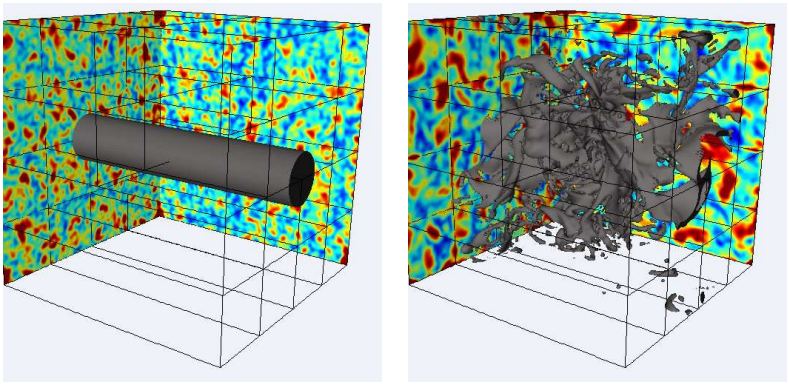

(a) $tu'/L_{\mathrm{int}} = 0$ (b) $tu'/L_{\mathrm{int}} = 1$

Fig. 10: Snapshots of the interface and vorticity fields in a periodic box for $r = \rho_l/\rho_g = 10$ and $\mathrm{Re}_L = 375$. Grid: 128^3 cells.

Because no surface tension force is included, the dense phase quickly desintegrates in small fragments that are advected around the box (Figure 10(b)). Figure 11(a) depicts the energy decay for single flow as well as the energy decays obtained for a density ratio 10 and 1000. As expected, all situations recover the same energy decay irrespective of the density ratio and despite the appearance of small under-resolved structures. The differences are more appreciable looking at higher order statistics such as the Taylor scale (Figure 11(b)). The reason from this departure is attributed to the presence of small droplets that can not be correctly resolved. As observed in the histrogram included in Figure 12, there is a quick disintegration of the liquid rim for $tu'/L_{\mathrm{int}} > 1$ that impedes an accurate solution of the equations. In any event, we remark that the errors induced by the under-resolved structures are negligible in terms of energy dissipation and are still in relative good agreement for the Taylor scale.

4.5.3 Energy decay in isotropic turbulence with multiple phases in the presence of surface tension effects

In this section we consider the same example as above but including surface tension. Figure 13 depicts the snapshot of the interface at $tu'/L_{\mathrm{int}} = 1$ when $r = \rho_l/\rho_g = 10$ and the Weber number is

$$\mathrm{We} = \frac{\rho_l (u')^2 R}{\sigma} = 1. \tag{49}$$

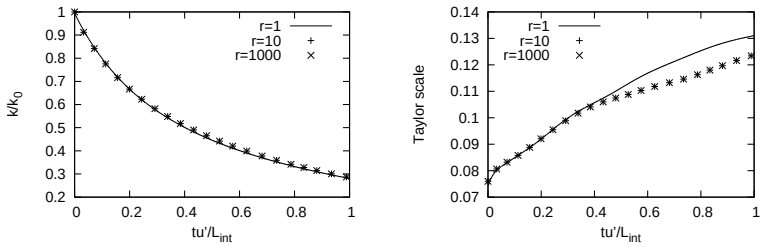

(a) Kinetic energy (b) Taylor microscale

Fig. 11: Temporal evolution of the system kinetic energy and Taylor scale as a function of the density ratio r for $\mathrm{Re}_L = 375$.

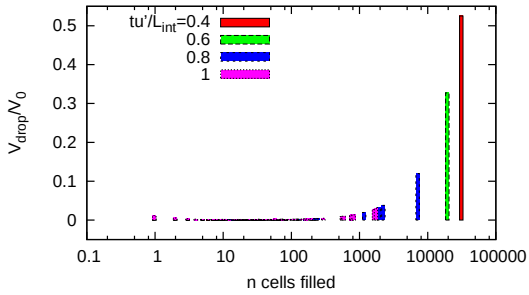

Fig. 12: Histogram of the PDF droplet distribution obtained for $r = \rho_l/\rho_g = 10$ and $\mathrm{Re}_L = 375$ at different dimensionless times. The x-axis represents the number of *filled* cells used to resolve a given droplet. The y-axis contains the volume ratio between the droplet and the initial rim volume.

Due to the small Weber number, the interface is no longer controlled by the dynamics of the turbulent flow but by surface tension effects. The initial turbulence level induces perturbations at the interface that triggers the Plateau-Rayleigh instability. As shown in Figure 13, we do need to significantly increase the level of refinement in order to capture the correct evolution of the interface with respect to that required to perform the DNS of single phase flows. In terms of turbulent statistics, the energy decay depicted in Figure 14(a) reveals that this magnitude is not significantly influenced neither by the dynamics of the interface nor by the level of resolution, recovering for all cases the same energy decay than that obtained for single phase flows. The reason is that the variations of the potential energy associated to the surface tension force during the simulation are small compared to the system's kinetic energy. In fact, the ratio between the potential energy stored initially at the interface and the intial

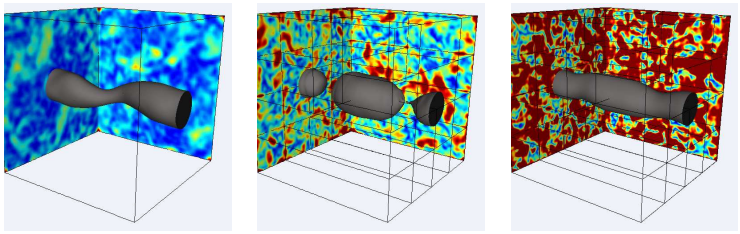

(a) 64^3 (b) 128^3 (c) 256^3

Fig. 13: Snapshots at $tu'/L_{\text{int}} = 1$ of the interface and vorticity fields in a periodic box for three different levels of refinement. $r = \rho_l/\rho_g = 10$, $\text{We} = 1$ and $\text{Re}_L = 375$.

system's kinetic energy is already relatively small,

$$\frac{A_{\text{cylinder}}\sigma}{E_k V_{\text{box}}} = 0.126. \tag{50}$$

When we look at higher order moments (Figure 14(b)) we do observe significant changes on the Taylor microscale as soon as the pinch-off of the liquid rim occurs. In the example considered here, the pinch-off of the interface is only observed at around $tu'/L_{\text{int}} = 0.8$ in the simulation with 128^3 grid points, which induces a strong deviation on the prediction of the Taylor scale evolution with that compared to single phase flows. When no pinch-off is observed, the evolution of the high order statistics is not significantly influenced by surface tension and we obtain a similar temporal evolution of the Taylor scale than that obtained for single phase flows.

We can conclude then that for $\text{We} \approx 1$ is important to correctly capture the interface dynamics if we want to reproduce higher order statics, but not other quantities such as the energy decay. In the first case, we find that the level of refinement required to obtain an accurate representation of the interface can be significantly larger than that needed to resolve the turbulent scales of the flow. Thus, this scenario seems a good candidate to apply dynamic mesh refinement techniques in order to save computational time. The investigation of the performance of AMR techniques in these flows is currently under research.

5 Conclusions

This paper presents a new numerical scheme oriented towards the simulation of turbulent multiphase flows. The scheme is based on a skew-symmetric formulation for the discretization of the Navier-Stokes equations that preserves energy in the discrete form in absence of any physical source of energy dissipation.

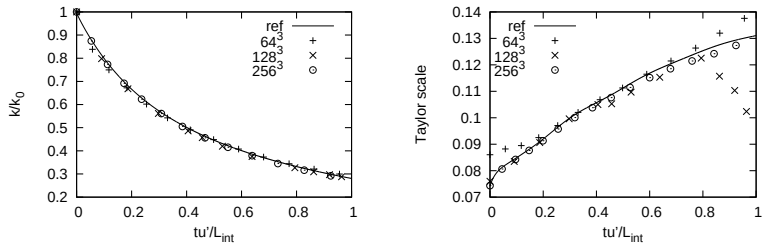

(a) Kinetic energy (b) Taylor microscale

Fig. 14: Temporal evolution of the system kinetic energy and Taylor scale for $r = \rho_l/\rho_g = 10$, We $= 1$ and $\mathrm{Re}_L = 375$.

This algorithm, initially presented by Verstappen et al [33], is extended here for systems with multiple phases with different densities and viscosities. Surface tension terms have been also incorporated into the formulation, paying especial attention in order to minimize the appearance of *parasitic* currents induced by surface tension.

The numerical tests shown in this manuscript indicate that the new formulation is especially suitable for the simulation of multiphase flows at low resolution, where the code provide comparable results in terms of accuracy than previous schemes presented by [23] for the simulation of multiphase flows. The main advantage of the new formulation is that it only requires one projection per timestep, which increases the speed of the code, and preserves energy for inviscid fluids.

References

[1] Energy-bounded flow approximation on a cartesian-product grid over rough terrain. *Journal of Computational Physics*, 107(1):51 – 65, 1993.

[2] A. Bagué, D. Fuster, S. Popinet, R. Scardovelli, and S. Zaleski. Instability growth rate of two-phase mixing layers from a linear eigenvalue problem and an initial value problem. *Physics of Fluids*, 22(9), 2010.

[3] J.B. Bell, P. Colella, and H.M. Glaz. A second-order projection method for the incompressible navier-stokes equations. *J. Comput. Phys.*, 85:257–283, 1989. single vortex test.

[4] A.J. Chorin. On the convergence of discrete approximations to the Navier–Stokes equations. *Mathematics of Computation*, 23(106):341–353, 1969.

[5] S. Chumakov. http://code.google.com/p/hit3d/.

[6] SG Chumakov. Gravitational effects in reactive flows: from physics to large eddy simulation modeling. *ADTSC Nuclear Weapons Program Highlights, Los Alamos National Laboratory (unclassified)*, 2007.

[7] SG Chumakov. A priori study of subgrid-scale flux of a passive scalar in turbulence. *Phys. Rev. E*, 78:15563, 2008.

[8] O. Desjardins and V. Moureau. Methods for multiphase flows with high density ratio. Center for Turbulence Research, 2010. Proceedings of the Summer Program 2010.

[9] O. Desjardins, V. Moureau, and H. Pitsch. An accurate conservative level set/ghost fluid method for simulating turbulent atomization. *J. Comput. Phys.*, 227:8395 – 8416, 2008.

[10] F. Ducros, F. Laporte, T. Souleres, V. Guinot, P. Moinat, and B. Caruelle. High-order fluxes for conservative skew-symmetric-like schemes in structured meshes: application to compressible flows. *Journal of Computational Physics*, 161(1):114–139, 2000.

[11] S. Elgobashi. An updated classification map of particle-laden turbulent flows. In *IUTAM Symposium on Computational Approaches to Multiphase Flow*, pages 3–10. Springer, 2006.

[12] M. M. Francois, Cummins S. J., Dendy E. D., Kothe D. B., Sicilian J. M., and Williams M. W. A balanced-force algorithm for continuous and sharp interfacial surface tension models within a volume tracking framework. *Journal of Computational Physics*, 213:141–173, 2006.

[13] D. Fuster, G. Agbaglah, C. Josserand, S. Popinet, and S. Zaleski. Numerical simulation of droplets, bubbles and waves: state of the art. *Fluid Dynamics Research*, 41:065001, 2009.

[14] D. Fuster, A. Bagué, T. Boeck, L. Le Moyne, A. Leboissetier, S. Popinet, P. Ray, R. Scardovelli, and S. Zaleski. Simulation of primary atomization with an octree adaptive mesh refinement and VOF method. *International Journal of Multiphase Flow*, 35:550–565, 2009.

[15] A.E. Honein and P. Moin. Higher entropy conservation and numerical stability of compressible turbulence simulations. *Journal of Computational Physics*, 201(2):531–545, 2004.

[16] JC Kok. A high-order low-dispersion symmetry-preserving finite-volume method for compressible flow on curvilinear grids. *Journal of Computational Physics*, 228(18):6811–6832, 2009.

[17] R.J. LeVeque. *Finite volume methods for hyperbolic problems*. Cambridge university press, 2002.

[18] T. Manteuffel and JR White, A. B. The numerical solution of second-order boundary value problems on nonuniform meshes. *Mathematics of Computation*, 47(176):511–535, 1986.

[19] J. Meyers, B.J. Geurts, and M. Baelmans. Database analysis of errors in large-eddy simulation. *Physics of Fluids*, 15:2740, 2003.

[20] S.B. Pope. *Turbulent flows*. Cambridge Univ Pr, 2000.

[21] S. Popinet. http://gfs.sourceforge.net/wiki/index.php.

[22] S. Popinet. Gerris: a tree-based adaptive solver for the incompressible Euler equations in complex geometries. 190(2):572–600, 2003.

[23] S. Popinet. An accurate adaptive solver for surface-tension-driven interfacial flows. *Journal of Computational Physics*, 288:5838–5866, 2009.

[24] M. Raessi and H. Pitsch. Consistent mass and momentum transport for simulating incompressible interfacial flows with large density ratios using the level set method. *Computers and Fluids*, 63:70–81, 2012.

[25] Y. Renardy and M. Renardy. Prost: A parabolic reconstruction of surface tension for the volume-of-fluid method. *J. Comput. Phys.*, 183:400–421, 2002.

[26] W. J. Rider. Approximate projection methods for incompressible flows: Implementation, variants and robustness. Technical report, Los Alamos National Laboratory (LA-UR-2000), 1995.

[27] O. Simonin. Continuum modelling of dispersed two-phase flows. *Lecture series-van Kareman Institute for fluid dynamics*, 2:K1–K47, 1996.

[28] M. Sussman and M. Ohta. Improvements for calculating two-phase bubble and drop motion using an adaptive sharp interface method. *Fluid Dyn. Mater. Process*, 3(1):21–36, 2007.

[29] G. Tomar, D. Fuster, S. Zaleski, and S. Popinet. Multiscale simulations of primary atomization using gerris. *Comp. and Fluids*, 39(4):1864–1874, 2010.

[30] E.F. Toro. *Riemann solvers and numerical methods for fluid dynamics- A practical introduction*. Berlin: Springer-Verlag, 1997.

[31] D.J. Torres and J.U. Brackbill. The point-set method: front-tracking without connectivity. *Journal of Computational Physics*, 165(2):620–644, 2000.

[32] G. Tryggvason, R. Scardovelli, and S. Zaleski. *Direct Numerical Simulations of Gas-Liquid Multiphase Flows*. Cambridge University Press, 2011.

[33] R. Verstappen and A.E.P. Veldman. Symmetry-preserving discretization of turbulent flow. *Journal of Computational Physics*, 187(1):343–368, 2003.

[34] R. Verstappen and AEP Veldman. Preserving symmetry in convection-diffusion schemes. *Turbulent flow computation*, pages 75–100, 2004.